PPARG directs trophoblast cell fate and establishment of the uterine-placental interface

Esteban M. Dominguez[1,*], Ayelen Moreno-Irusta[1], Khursheed Iqbal[1ψ], Keting Chen[2], Alex Finlinson[3], Marc Parrish[3], Hiroaki Okae[4], Takahiro Arima[5], Geetu Tuteja[2], and Michael J. Soares[1,3,*]

[1]Institute for Reproductive and Developmental Sciences, Department of Pathology & Laboratory Medicine, University of Kansas Medical Center, Kansas City, KS 66160, [2]Department of Genetics, Development, and Cell Biology, Iowa State University, Ames, IA 50011,[3]Department of Obstetrics and Gynecology, University of Kansas Medical Center, Kansas City, KS 66160,[4]Department of Trophoblast Research, Institute of Molecular Embryology and Genetics, Kumamoto University, Kumamoto 860-0811, Japan,[5]Department of Informative Genetics, Environment and Genome Research Center, Tohoku University Graduate School of Medicine, and Department of Molecular Oncology, Institute of Development, Aging and Cancer, Tohoku University, Sendai 980-8575, Japan

[ψ]Present address: Department of Animal & Food Science, Oklahoma State University, Stillwater, OK, 74078.

***Corresponding authors:** Esteban M. Dominguez, edominguez@kumc.edu or Michael J. Soares, msoares@kumc.edu

3901 Rainbow Blvd. Kansas City, KS 66160, Mail Stop 3050.

Phone: 913 588 5960 or 913 588 5961.

Abstract

The expansion and differentiation of trophoblast stem (**TS**) cells are critical for defining fundamental properties of the placenta. Specialized trophoblast cells exit the placenta and enter and transform the uterus, including restructuring uterine spiral arteries. In the human these cells are referred to as extravillous trophoblast (**EVT**) cells, whereas in the rat they are termed invasive trophoblast cells. Mechanisms governing invasive trophoblast cell differentiation remain poorly understood. We investigated peroxisome proliferator-activated receptor gamma (**PPARG**) as a potential regulator of EVT/invasive trophoblast cell development. In first trimester human placentas, PPARG transcripts and protein were detected in the EVT cell column and increased in amount as human TS cells differentiated into EVT cells. Disruption of PPARG impaired differentiation of human TS cells into EVT cells. Invasive trophoblast cells of the rat placentation site similarly expressed PPARG. Conditional inactivation of PPARG within invasive trophoblast cells of the rat placenta was used to assess the in vivo role of PPARG on the uterine-placental interface. PPARG was established as an essential cell-autonomous regulator of the invasive trophoblast cell lineage with profound effects on placentation. In conclusion, PPARG is a conserved regulator of placentation and is essential for directing trophoblast cell-guided uterine transformation.

Keywords: PPARG, trophoblast cell invasion, hemochorial placenta.

Introduction

The uterine-placental interface is a dynamic site where uterine and placental structures cooperate to establish a protective environment that redirects maternal resources to support embryonic and fetal development (Georgiades et al. 2002; Maltepe and Fisher 2015). Both humans and rats possess a hemochorial placenta, characterized by deep trophoblast cell invasion into the uterine parenchyma and remodeling of the uterine vasculature to ensure optimal maternal blood supply to the placenta (Pijnenborg et al. 1981; Soares et al. 2012). This vascular transformation is critical for successful pregnancy (Pijnenborg et al. 2006; Aye et al. 2025). Impairments in this process can lead to complications such as pregnancy loss, preeclampsia, intrauterine growth restriction, and preterm birth (Aye et al. 2025; Brosens et al. 2011; Fisher 2015; Brosens et al. 2019; Harris et al. 2019). These complications significantly contribute to maternal and fetal morbidity and mortality (Fisher 2015; Brosens et al. 2019; Kaufmann et al. 2003). Furthermore, suboptimal intrauterine conditions can trigger fetal adaptations that increase susceptibility to disease later in life (Calkins and Devaskar 2011; Gluckman et al. 2008).

Throughout gestation, maternal blood flows into the placenta, delivering essential nutrients and oxygen to support fetal development. As pregnancy progresses, maternal uterine spiral arteries are remodeled into distended, low-resistance vessels capable of meeting the increasing demands of the growing fetus (Kaufmann et al. 2003; Harris 2010). At the core of spiral artery remodeling are invasive trophoblast cells, referred to as extravillous trophoblast (**EVT**) cells in humans (Velicky et al. 2015). These cells take two routes into the uterus. They migrate inside the uterine vasculature and within the uterine stroma situated between uterine blood vessels and are referred to as endovascular invasive trophoblast/EVT cells and interstitial invasive trophoblast/EVT cells, respectively. Endovascular invasive trophoblast/EVT cells replace endothelial cells and adopt a pseudo-endothelial phenotype (Hemberger et al. 2003; Rai and Cross 2014). Given the critical role of invasive trophoblast/EVT cells in uterine spiral artery

68 remodeling, it is crucial to identify mechanisms that regulate invasive trophoblast/EVT cell
69 development.
70
71 Peroxisome proliferator-activated receptor gamma (**PPARG**) is a member of the nuclear
72 hormone receptor superfamily of ligand-activated transcription factors (Sauer 2015). PPARG is
73 essential for placental development in the mouse (Barak et al. 1999; Kubota et al. 1999).
74 Deficiency of PPARG results in embryonic lethality at mid-gestation (Barak et al. 1999; Kubota et
75 al. 1999). In addition, PPARG is expressed in the human placenta and is involved in human
76 trophoblast cell development and regulating key placental functions (Schaiff et al. 2006; Tarrade
77 2001; Tarrade et al. 2001; Pavan et al. 2003; Fournier et al. 2007; Schaiff et al. 2000; Shalom-
78 Barak et al. 2004). Among its diverse actions on placentation is its potential involvement in
79 regulating the invasive trophoblast cell lineage. Within rat and human placentation sites, PPARG
80 is prominently expressed in invasive trophoblast/EVT cell lineages (Liu et al. 2018; Vento-Tormo
81 et al. 2018; Scott et al. 2022). PPARG dysregulation is also evident in diseases associated with
82 failures in trophoblast cell-guided uterine spiral artery remodeling such as preeclampsia and
83 intrauterine growth restriction (Rodie et al. 2005; Waite et al. 2005; Holdsworth-Carson et al.
84 2010).
85
86 In this study, we investigated the involvement of PPARG on EVT cell lineage development in
87 vitro using human trophoblast stem (**TS**) cells. Human TS cells are a robust in vitro model system
88 and have provided new insights into the regulation of trophoblast cell differentiation (Okae et al.
89 2018; Varberg et al. 2023). The contributions of PPARG to invasive trophoblast cell development
90 were also examined in vivo using a conditionally disrupted *Pparg* rat model. Our findings
91 demonstrate that PPARG is a critical and conserved regulator of invasive trophoblast cell
92 development and invasive trophoblast cell-guided transformation of the uterine vasculature.

Results

PPARG is expressed in EVT cells

Distributions of PPARG transcript and protein in first trimester human placenta tissue were determined by in situ hybridization and immunohistochemistry, respectively. PPARG transcript (Fig. 1A) and protein (Fig. 1B) were ubiquitously expressed throughout trophoblast cells within villous and extravillous compartments of the human placenta, including EVT cells. The transcript for notum, palmitoleoyl protein carboxylesterase (**NOTUM**), an EVT cell-associated marker (Shukla et al. 2024), co-localized with PPARG transcripts in the distal region of the EVT cell column (Fig. 1A). PPARG protein was located within nuclei of EVT cells (Fig. 1B). These observations are consistent with previous reports (Tarrade et al. 2001; Waite et al. 2000). PPARG expression was also examined in CT27 (X,X) human TS cells. TS cells can be maintained in the stem state or induced to differentiate into EVT cells (Okae et al. 2018). Expression of *TEAD4* and *TP63* defined the stem state of these cells, whereas *HLA-G* and *MMP2* characterized EVT cell differentiation (Supplemental Fig. S1A). PPARG transcript and protein expression increased from the stem state to day 8 of EVT cell differentiation (Fig. 1C). Thus, PPARG is expressed in EVT cells of the developing human placenta and in human TS cells induced to differentiate into EVT cells.

PPARG effects on EVT cell differentiation

The expression of PPARG within EVT cells prompted an investigation into a possible role for PPARG in EVT cell development. A lentiviral-mediated short hairpin RNA (**shRNA**) loss-of-function strategy was used to inhibit PPARG in CT27 TS cells. PPARG transcript and protein were significantly decreased in TS cells stably expressing a PPARG shRNA and induced to differentiate into EVT cells when compared to expression of a control shRNA (Fig. 2A). Treatment with the PPARG shRNA slowed TS cell proliferation without changes in stem sate associated markers TEAD4 and TP63 (Supplemental Fig. S1B-D). Disruption of PPARG affected the morphology of the EVT cell differentiation state, including a decrease in cell elongation and the presence of stem state-like cell clusters (Fig. 2B). Cells expressing PPARG shRNAs showed significantly less migration than EVT cells expressing control shRNAs (Fig. 2C). Similar findings were observed in

121 CT29 (X,Y) TS cells following their manipulation with PPARG shRNA (Supplemental Fig. S2A-C).
122 Additionally, exposure to a small molecule PPARG antagonist (GW9662) similarly negatively
123 affected stem state proliferation, EVT cell differentiation, and cell migration (Supplemental Fig.
124 S3A-J**)**. Collectively, the findings indicate that PPARG possesses a fundamental role in regulating
125 EVT cell development and function.
126
127 *PPARG effects on trophoblast organoids*
128 We next examined the involvement of PPARG in establishment and behavior of TS cell-derived
129 trophoblast organoids. We initially validated the TS cell-derived trophoblast organoid culture
130 system (Supplemental Fig. S4A–D) and then examined control or PPARG deficient trophoblast
131 organoids. The ability to form trophoblast organoids was not affected by PPARG disruption (Fig.
132 3A); however, PPARG inhibition did affect EVT cell differentiation from trophoblast organoids (Fig.
133 3B). This finding was supported by inspection of the morphology of the trophoblast organoids and
134 their expression of TS cell stem state transcripts (*TEAD4, TFAP2C, TP63, CDH1*) and EVT cell-
135 associated transcripts (*MMP15, HLA-G, FSTL3, ASCL2, DLX6, PLAC8*) (Fig. 3C).
136
137 *Identification of PPARG gene targets in EVT cells*
138 PPARG is a transcription factor, which prompted an examination of transcripts affected by
139 PPARG disruption. RNA sequencing (**RNA-seq**) was performed, and transcriptomic profiles
140 analyzed following eight days of EVT cell differentiation in control shRNA and PPARG shRNA
141 treated cells (Supplemental Dataset 1**)**. A total of 5,845 differentially expressed genes were
142 identified in control versus PPARG shRNA treated cells ($p<0.05$, and fold change of 1.5), including
143 2,510 upregulated and 3,335 downregulated genes. The differential gene expression profile is
144 presented as a volcano plot (Fig. 4A). Selected upregulated and downregulated genes connected
145 to trophoblast cell biology are shown in a heat map (Fig. 4B). We identified upregulation of several
146 genes associated with the TS cell stem state (e.g. *TEAD4, TFAP2C, TP63, CDH1*) and
147 downregulation of several EVT cell-associated genes (e.g. *ITGA1, ITGAV, FLT1, EPAS1, DLX6,*
148 *PLAC8, TFPI, FSTL3*). These findings were independently validated by reverse transcriptase-

149 quantitative polymerase chain reaction (**RT-qPCR,** Fig. 4C, Supplemental Fig. S5**).** Gene ontology
150 (**GO**) (Fig. 4D and Supplemental Dataset S2 and S3) and gene set enrichment analysis (**GSEA**)
151 (Fig. 4E and Supplemental Dataset S4) implicated PPARG in the upregulation of cell cycle
152 associated genes and the downregulation of cell projection assembly associated genes. The latter
153 cellular process directly connects PPARG with cell elongation and motility that are acquired as TS
154 cells transit from the stem state to EVT cells.
155
156 Since, PPARG acts by binding to DNA and coordinating the regulation of gene transcription,
157 we next examined the genome-wide profile of PPARG-DNA interactions using chromatin
158 immunoprecipitation sequencing (**ChIP-seq**). We identified 7,319 genes with at least one PPARG
159 bound region (peak) in differentiated EVT cells (Supplemental Dataset S5). The two most prevalent
160 motifs identified within the peaks were known PPARG DNA binding motifs (peroxisome proliferator
161 response element, **PPRE**) and primarily consisted of a direct repeat 1 (**DR1**) sequence (Fig. 5A).
162 Most of PPARG-DNA peaks (~7000) were located within introns or intergenic regions of protein-
163 coding genes (Fig. 5B and C), suggesting the involvement of PPARG in the regulation of enhancer
164 activity. Integration of RNA-seq (5,845 differentially expressed genes) and ChIP-seq (7,319 genes
165 with PPARG peak) datasets resulted in the identification of 2,512 potential direct PPARG gene
166 targets (Fig. 5D, Supplemental Dataset S6). GO analyses of PPARG gene targets identified by
167 PPARG ChIP-seq (Fig. 5E, Supplemental Dataset S7) and an integrated dataset of PPARG
168 responsive genes identified by RNA-seq of EVT cells (see Fig. 4) and PPARG gene targets
169 identified by PPARG ChIP-seq (Fig. 5F, Supplemental Dataset 8) prominently identified genes
170 associated with positive regulation of cell projection organization and tissue migration. These
171 represent cellular processes associated with EVT cell differentiation. Evidence supporting *PLAC8*,
172 *TFPI*, *DLX6*, *FSTL3* and *TP63*, which are known regulators of trophoblast cell differentiation (Chang
173 et al. 2018; Xie et al. 2018; Muto et al. 2021; Wang et al. 2022; Kim et al. 2024), as potential direct

174 targets of PPARG is shown (Fig. 5G**)**. Collectively, the results support PPARG regulating genes
175 that control development of the EVT cell lineage.
176
177 *PPARG expression within the rat uterine-placental interface*
178 The rat exhibits deep intrauterine trophoblast cell invasion (Ain et al. 2003), a feature of
179 placentation also observed in the human, and has proven to be a useful in vivo model for
180 investigating the physiological relevance of genes implicated in the regulation of the invasive
181 trophoblast cell lineage (Chakraborty et al. 2016; Varberg et al. 2021; Muto et al. 2021; Kuna et al.;
182 Dominguez et al. 2024). We next sought to determine whether PPARG was expressed in
183 trophoblast cells of the rat placenta, especially within invasive trophoblast cells of the rat uterine-
184 placental interface. The rat placentation site is organized into three main compartments: i) labyrinth
185 zone, ii) junctional zone, and iii) uterine-placental interface (Soares et al. 2012; Shukla and Soares
186 2022). The labyrinth zone is comprised of trophoblast cells and fetal vasculature and represents
187 the site of maternal-fetal exchange, whereas the junctional zone contains several trophoblast cell
188 types, including invasive trophoblast cell progenitors, which direct pregnancy-dependent
189 adaptations of maternal tissues. The uterine-placental interface is the uterine compartment
190 adjacent to the placenta where invasive trophoblast cells, uterine vasculature, and maternal
191 immune cells are situated. *In situ* hybridization was used to determine the distribution of *Pparg*
192 transcripts. At gestation day (**gd**) 11.5, *Pparg* transcripts were localized to trophoblast cells of the
193 developing placenta as well as to invasive trophoblast cells situated within uterine spiral arteries
194 (Fig. 6A). The presence of *Pparg* transcripts in trophoblast cells was confirmed by co-localization
195 with keratin 8 (*Krt8*), an epithelial cell associated transcript expressed by trophoblast cells (Fig. 6A).
196 By gd 18.5, *Pparg* was expressed within trophoblast cells of the labyrinth zone, junctional zone,
197 and within invasive trophoblast cells of the uterine–placental interface (Fig. 6B). Expression of
198 *Pparg* in invasive trophoblast cells was supported by its co-localization with prolactin family 7,
199 subfamily b, member 1 (***Prl7b1*,** Fig. 6B), an invasive trophoblast cell-associated transcript (Scott
200 et al. 2022; Wiemers et al. 2003). These findings are consistent with a previously published report
201 describing single cell RNA-seq analysis of the rat uterine–placental interface, which demonstrated

202 that *Pparg* expression was enriched in the invasive trophoblast cell lineage (Supplemental Fig. S6)
203 (Scott et al. 2022). *Pparg* transcript levels increased within the uterine–placental interface as
204 pregnancy progressed (Fig. 6C). Furthermore, PPARG protein was localized to invasive
205 trophoblast cells and throughout the junctional and labyrinth zones, as shown by
206 immunohistochemistry (Fig. 6D). Thus, PPARG expression is a conserved feature of EVT cells of
207 the human placenta (Fig. 1) and invasive trophoblast cells of the rat placentation site (Fig. 6).
208

209 *Establishment and validation of the invasive trophoblast cell-specific Pparg mutant rat*

210 Next, we examined an in vivo role for PPARG in development of rat invasive trophoblast cells.
211 Since, PPARG is expressed in trophoblast cell lineages throughout the rat placentation site (Fig.
212 6B) and global inactivation of the mouse *Pparg* gene was associated with midgestation lethality
213 (Barak et al. 1999; Kubota et al. 1999), we utilized a conditional Cre/Lox approach to selectively
214 disrupt *Pparg* in the invasive trophoblast cell lineage. Male *Prl7b1-Cre* rats, specifically expressing
215 *Cre* recombinase in the invasive trophoblast cell lineage (Dominguez et al. 2024; Iqbal et al. 2024)
216 and female rats possessing *loxp* sites flanking Exons 2 and 3 of the *Pparg* gene (Fig. 7A) were
217 used in the analysis. Specifically, *Prl7b1-Cre*/heterozygous floxed *Pparg* (***Prl7b1^{Cre}/Pparg$^{f/+}$***) males
218 were mated with homozygous floxed *Pparg* female rats (***Pparg$^{f/f}$***) to generate *Pparg$^{f/f}$* and *Pparg*
219 deleted (***Pparg$^{d/d}$***) placentation sites. Immunohistochemical analysis for PPARG demonstrated the
220 presence of PPARG protein at the gd 18.5 uterine–placental interface of *Pparg$^{f/f}$* but not *Pparg$^{d/d}$*
221 placentation sites (Fig. 7B).
222

223 *PPARG involvement in rat invasive trophoblast cell lineage development and cellular dynamics*
224 *within the uterine-placental interface*

225 The structure and integrity of *Pparg$^{f/f}$* and *Pparg$^{d/d}$* placentation sites were different. *Pparg$^{d/d}$*
226 placentas were larger (Fig. 7C), possessed an expanded junctional zone (Supplemental Fig. S7)
227 containing prominent cyst-like structures (Fig. 7C), and were less efficient than *Pparg$^{f/f}$* placentas
228 (Fig. 7D**)**. Invasive trophoblast cells arise from the junctional zone (Soares et al. 2012; Shukla and

229 Soares 2022) and exhibited pronounced differences between *Pparg*$^{f/f}$ and *Pparg*$^{d/d}$ placentation
230 sites (Fig. 8).
231
232 The uterine-placental interface of *Pparg*$^{f/f}$ placentation sites was infiltrated with invasive
233 trophoblast cells, which was not observed in *Pparg*$^{d/d}$ placentation sites, as detected by in situ
234 hybridization for *Prl7b1* or pan-cytokeratin immunostaining (Fig. 8A and B). Deficits in intrauterine
235 trophoblast cell invasion correlated with diminished expression of invasive trophoblast cell-
236 associated transcripts (*Prl5a1*, *Prl7b1*, *Krt8, Krt7, Cited2, Peg3, and Tfpi*) and pan-cytokeratin
237 immunoreactive surface area within the uterine-placental interfaces of *Pparg*$^{d/d}$ placentation sites
238 (Fig. 8C and D, Supplemental Fig. S8). Previously published single cell RNA-sequencing and single
239 nucleus assay for transposase-accessible chromatin-sequencing datasets (Scott et al. 2022; Vu et
240 al. 2023) were used to reveal a network of genes potentially regulated by PPARG in rat invasive
241 trophoblast cells. These putative PPARG targets include candidate contributors to remodeling the
242 extracellular matrix, regulation of cell movement, cytoskeletal restructuring, and transcriptional
243 regulators that act on genes encoding other proteins affecting the invasive trophoblast cell
244 phenotype (Supplemental Table S1 and Supplemental Dataset S9).
245
246 Diminished intrauterine trophoblast cell invasion in *Pparg*$^{d/d}$ placentation sites was
247 accompanied by a retention of natural killer (**NK**) cells within the uterine-placental interface (Fig.
248 8E) and increased expression of NK cell-associated transcripts (Fig. 8F). NK cells are known
249 contributors to uterine spiral artery remodeling (Chakraborty et al. 2011; Rätsep et al. 2015; Renaud
250 et al. 2017; Erlebacher 2013) but were less effective than invasive trophoblast cells in disabling

251 smooth muscle cells associated with uterine spiral arteries than invasive trophoblast cells (Fig. 8G
252 and H).
253
254 Overall, these results highlight a key role for PPARG in directing development of the invasive
255 trophoblast cell lineage and the important role that invasive trophoblast cells possess in regulating
256 the cell composition and function of the uterine-placental interface.
257
258 **Discussion**
259 Hemochorial placentation serves the important function of delivering nutrients to ensure
260 coordinated on-time growth and development of the fetus within the female reproductive tract
261 (Soares et al. 2018). This type of placentation is found in many primates and rodents, including
262 the human and rat (Carter and Enders 2004; Roberts et al. 2016). These two species exhibit
263 extensive invasive trophoblast cell-guided uterine transformation, including restructuring of spiral
264 arteries, which is fundamental to acquisition of maternal resources required for fetal development
265 (Pijnenborg et al. 1981). We examined a role for PPARG in development of invasive trophoblast
266 cells using human TS cells and a genetically manipulated rat model. In human placentation,
267 PPARG was expressed in EVT cell column cells and was shown to coordinate the upregulation of
268 genes required for cell elongation and the process of EVT cell movement. In the rat, PPARG was
269 expressed throughout the placenta, including invasive trophoblast cells, and was essential for
270 development of the invasive trophoblast cell lineage. Failures in PPARG-mediated gene
271 activation also affected human TS cell proliferation and led to abnormalities within compartments
272 of the rat placenta. The experimentation demonstrated that PPARG is a conserved regulator of
273 invasive trophoblast cell development and function.
274
275 Earlier research connected PPARG to placentation (Schaiff et al. 2006; Fournier et al. 2011;
276 Kadam et al. 2015). Insights regarding PPARG actions in placentation were unequivocally
277 demonstrated from analysis of global PPARG null mouse models (Barak et al. 1999; Kubota et al.
278 1999). PPARG disruption led to midgestation lethality due to an impairment of early events in

279 placental morphogenesis (Barak et al. 1999; Kubota et al. 1999). Considerable effort has also
280 been directed towards analyses of roles for PPARG in regulating trophoblast cells using an
281 assortment of in vitro models. PPARG deficient mouse TS cells exhibit impairments in
282 proliferation and syncytiotrophoblast development and enhanced trophoblast giant cell
283 differentiation (Parast et al. 2009), whereas human cytotrophoblast exposure to PPARG agonists
284 promoted syncytiotrophoblast formation and trophoblast cell-lipid accumulation, while inhibiting
285 trophoblast cell invasive properties (Tarrade 2001; Tarrade et al. 2001; Schaiff et al. 2005). Our in
286 vitro and in vivo experimentation supported an essential role for PPARG in EVT/invasive
287 trophoblast cell lineage development. Similar observations of the involvement of PPARG in EVT
288 cell differentiation have recently been reported (Guo et al. 2025). Exposure to a PPARG
289 antagonist supported the involvement of PPARG actions in promoting EVT cell differentiation.
290 These PPARG actions on the EVT/invasive trophoblast cell lineage differ from observations with
291 PPARG activating ligands. PPARG can act independent of ligand and its actions can vary
292 depending upon the ligand investigated and may differ depending on the developmental state of
293 the target cells examined (Sauer 2015). Thus, PPARG is a broad-spectrum regulator of placental
294 biology with critical actions on development of the EVT/invasive trophoblast cell lineage.
295
296 As indicated above, PPARG is expressed in multiple trophoblast cell lineages (Barak et al.
297 1999; Tarrade 2001; Fournier et al. 2007; Waite et al. 2005; Asami-Miyagishi et al. 2004). Each
298 trophoblast cell lineage is responsible for controlling tasks critical for the development and
299 function of the placenta (Soares et al. 2018). Context is important. PPARG actions are not only
300 determined by its presence but also by the complement of posttranslational modifiers,
301 heterodimerization binding partners, and co-regulators expressed by a cell (Berger and Moller
302 2002; Feige et al. 2006; Ahmadian et al. 2013).
303
304 In addition to PPARG, several other proteins have been shown to contribute to the regulation
305 of EVT cell differentiation. ASCL2, CITED2, DLX5, DLX6, EPAS1, GCM1, NOTUM, NRIP1,
306 SNAI1, TFAP2C, TFPI, WWTR1, and ZNF439, are required for optimal transition from the TS

307 cell stem state to EVT cells (Varberg et al. 2023; Shukla et al. 2024; Varberg et al. 2021; Muto et
308 al. 2021; Kuna et al.; Kim et al. 2024; Jeyarajah et al.; Meinhardt et al.). A *CRISPR* screen
309 identified additional transcription factors contributing to the regulation of human TS cells (Shimizu
310 et al. 2023). The screen demonstrated the involvement of PPARG in the control of TS cell
311 proliferation, which was consistent with our observations, but not EVT cell differentiation. The
312 *CRISPR* screen utilized HLA-G expression as a method for monitoring EVT cell differentiation.
313 PPARG does not significantly affect HLA-G gene expression, which may account for differences
314 in the outcome of the *CRISPR* screen versus our findings. Based on RNA-seq and ChIP-seq
315 experiments we can place PPARG in a potential hierarchy of transcription factors controlling EVT
316 cell development (Supplemental Fig. S9 (Varberg et al. 2023, 2021; Kuna et al.; Kim et al. 2024;
317 Jeyarajah et al.; Guo et al. 2025). Among the regulators impacting EVT cell differentiation,
318 ASCL2, TFPI, CITED2, TFAP2C and PPARG possess conserved actions promoting development
319 of the invasive trophoblast cell lineage in the rat (Varberg et al. 2021; Muto et al. 2021; Kuna et
320 al.; Dominguez et al. 2024).
321
322 PPARG deficiency was associated with failed trophoblast cell invasion into the uterus leading
323 to a dramatic reorganization of the rat placentation site. The reorganization included the retention
324 of NK cells within the uterine-placental interface and a disruption in the structural organization of
325 the two main placental compartments (junctional and labyrinth zones). NK cells are known
326 contributors to early events in uterine spiral artery remodeling (Chakraborty et al. 2011; Rätsep et
327 al. 2015; Renaud et al. 2017; Erlebacher 2013). NK cells vacate the uterine-placental interface as
328 invasive trophoblast cells enter the uterus (Ain et al. 2003). In addition to PPARG, TFAP2C is
329 also a driver of invasive trophoblast cell infiltration into the uterus (Dominguez et al. 2024).
330 Impairment of either PPARG or TFAP2C leads to failed intrauterine trophoblast cell invasion and
331 retention of NK cells within the uterine-placental interface. The implication is that invasive
332 trophoblast cells are engineering the exit of NK cells from the uterine-placental interface. In the
333 absence of invasive trophoblast cells, NK cells are supporting, at least partially, uterine spiral
334 artery remodeling and minimizing adverse pregnancy outcomes. The nature of the signal(s)

335 emanating from invasive trophoblast cells responsible for NK cell exodus is unknown.
336 Cooperation of invasive trophoblast cells and NK cells at the uterine-placental interface is robust.
337 It is expected that deficits in both maternal and extraembryonic contributions to uterine
338 transformation would exhibit more adverse consequences. In addition to the uterine-placental
339 interface, failure in the developmental progression of progenitor cells situated in the junctional
340 zone into invasive trophoblast cells resulted in malformations within the junctional zone. These
341 aberrations included the appearance of large cystic structures within the junctional zone and an
342 irregular junctional zone-labyrinth zone interface. Specific cellular dysfunctions linked to PPARG
343 deficiency underlying these structural defects in junctional zone morphogenesis are unknown.
344
345 Finally, PPARG transcriptional activity is influenced by the availability of glucose and lipids
346 (Berger and Moller 2002; Feige et al. 2006; Ahmadian et al. 2013). Thus, PPARG acts as a
347 nutrient sensor. Coupling nutrient sensing with the regulation of invasive trophoblast cell
348 transformation of the uterine vasculature would be an effective strategy for adapting to a nutrient-
349 variable maternal environment and is testable with the in vitro and in vivo models described in this
350 report.
351
352 **Materials and Methods**
353 *Human placentation site specimens*
354 Paraffin-embedded first-trimester placental tissue specimens were obtained from the
355 Lunenfeld-Tanenbaum Research Institute at Mount Sinai Hospital (Toronto, Canada). All tissue
356 samples were deidentified prior to use in this study. Tissue collection was conducted following
357 written informed consent and with approval from the Human Research Ethics Review Committees
358 at the University of Toronto and the University of Kansas Medical Center (**KUMC**).
359
360 *Human TS cell culture*
361 Human TS cells (CT27 and CT29) used in this study have been previously described (Okae
362 et al. 2018). The TS cells originated from deidentified first trimester human placental tissue

363 obtained from healthy women with signed informed consent and approval from the Ethics
364 Committee of Tohoku University School of Medicine. Experimentation with human TS cells was
365 approved by the KUMC Human Research Protection Program and the KUMC Human Stem Cell
366 Research Oversite committee. Human TS cell lines were maintained in the stem cell state and
367 differentiated into EVT cells as previously reported. Detailed culture conditions are provided in the
368 Supplemental Materials.
369
370 *Design and generation of lentiviral shRNA constructs*
371 PPARG shRNA sequences were designed and subcloned into the pLKO.1 vector at *AgeI* and
372 *EcoRI* restriction sites. shRNA sequences used in these analyses are listed in Supplemental
373 Table S2. Lentiviral packaging plasmids were obtained from Addgene and included pMDLg/pRRE
374 (plasmid 12251), pRSV-Rev (plasmid 12253), and pMD2.G (plasmid 12259). Lentiviral particles
375 were produced via transient transfection of the shRNA-pLKO.1 vector along with the packaging
376 plasmids into Lenti-X cells (632180, Takara Bio USA) using Attractene (301005, Qiagen) in Opti-
377 MEM I (51985-034, Thermo Fisher). Cells were maintained in Dulbecco's Modified Eagle Medium
378 (DMEM, 11995-065, Thermo Fisher) supplemented with 10% fetal bovine serum (**FBS**) for 24 h
379 prior to supernatant collection. At that point, cells were switched to Basal Human TS Cell
380 Medium. Conditioned medium containing viral particles was collected every 24 h over two days
381 and stored at −80 °C until used.
382
383 *Lentiviral transduction*
384 Human TS cells were plated at 65,000 cells per well in 6-well tissue culture-treated plates
385 coated with 5 µg/mL collagen IV (CB40233, Thermo Fisher) and incubated for 24 h. Prior to
386 transduction, medium was changed, and cells were incubated with 2.5 µg/mL polybrene for 30
387 min at 37°C. Following polybrene treatment, TS cells were transduced with 500 µL of conditioned
388 medium containing lentiviral particles and then incubated for 24 h. Medium was changed at 24 h
389 post transduction and selected with puromycin dihydrochloride (5 µg/mL, A11138-03, Thermo

390 Fisher) for 2 days. Cells recovered were cultured for 1 to 3 days in Complete TS Cell Medium and
391 then used to evaluate the effects of PPARG disruption on EVT cell differentiation.
392
393 *Cell migration assay*
394 Trophoblast cell migration was assessed according to the method described by Shimizu and
395 coworkers (Shimizu et al. 2023) with minor modifications. A suspension of 200,000 human TS
396 cells was prepared in Matrigel (100%) and Basal Human EVT Cell Differentiation Medium (10
397 μL). From this mixture, 1 μL was dispensed onto a 6-well plate to form individual Matrigel drops.
398 Six Matrigel drops were prepared. The drops were cultured in complete EVT cell differentiation
399 medium supplemented with 0.5% Matrigel (CB-40234, Thermo Fisher) at 37°C in a humidified
400 atmosphere containing 5% CO_2. Culture medium was replaced on day 3, and the cells were
401 incubated for a total of five days. EVT cells migrating from the cell aggregate were identified using
402 immunocytochemistry for HLA-G (1:300, phycoerythrin (**PE**)-labeled anti-HLA-G antibody,
403 ab24384, Abcam). After 15 min of incubation at 37°C, cells were fixed with 4% paraformaldehyde
404 (**PFA**). Nuclei were counterstained with 4',6-diamidino-2-phenylindole (**DAPI**, 1:50,000, D1306,
405 Invitrogen). Following washes with phosphate buffered saline (**PBS**, pH 7.4), the samples were
406 imaged using a Zeiss Axio Observer 7 microscope. The area of PE-labeled signal was quantified
407 using ImageJ software.
408
409 *Trophoblast organoids*
410 Human TS cells were used to establish trophoblast organoids as previously described
411 (Karvas et al. 2022) with minor modifications. Effects of PPARG on trophoblast organoid
412 formation and capacity to differentiate into EVT cells were determined. Detailed culture conditions
413 are provided in the Supplemental Materials.
414
415 *Animals and tissue collection*
416 Holtzman Sprague–Dawley rats were obtained from Envigo and used for in vivo experiments.
417 Animals were housed in an environmentally controlled facility under a 14-hour light/10-hour dark

418 lighting schedule with food and water available ad libitum. Timed pregnancies were established
419 by mating virgin female rats (8–10 weeks of age) with adult male rats (>3 months of age). Mating
420 was confirmed by the presence of sperm in the vaginal lavage, with the day of sperm detection
421 considered gd 0.5. Pseudopregnant females were generated by mating with vasectomized males,
422 and the presence of a seminal plug was designated as day 0.5 of pseudopregnancy. Pregnant
423 rats were euthanized at different days during gestation. Some placentation sites were frozen
424 intact in dry ice–cooled heptane and stored at –80 °C for subsequent histological analysis, while
425 other placentation sites were dissected into uterine–placental interface, junctional zone, and
426 labyrinth zone compartments, as previously describe (Ain et al. 2006).
427
428 *Conditional Pparg mutant rat*
429 In vivo *Pparg* disruption in invasive trophoblast cells was achieved using the Cre-loxP
430 system. LoxP cassettes were inserted into introns flanking Exons 2 and 3 of the *Pparg* locus
431 using *CRISPR*/Cas9 mediated homologous recombination (Fig. 5, Supplemental Table S3).
432 *CRISPR*/Cas9 reagents and templates were electroporated into one-cell rat embryos using a
433 NEPA21 electroporator (Nepa Gene), and embryos subsequently transferred to pseudopregnant
434 rats. Offspring were screened for mutations via polymerase chain reaction (**PCR**), and successful
435 loxP site insertion was confirmed by DNA sequencing (GeneWiz). A founder mutant animal was
436 backcrossed with wild-type rats to assess germline transmission. A *Prl7b1-Cre* recombinase rat
437 model was used to specifically disrupt *Pparg* in invasive trophoblast cells (Iqbal et al. 2024).
438
439 Genotyping and sex chromosome determinations were performed as previously described
440 (Dhakal and Soares 2017). Genomic DNA was extracted from tail-tip biopsies using the Red
441 Extract-N-Amp Tissue PCR Kit (XNAT-1000RXN, Sigma-Aldrich) and used for genotyping. Primer
442 sequences for detecting conditional mutations and determining sex chromosome composition are
443 provided (Supplemental Table S4).
444
445 *RT-qPCR*

446 Total RNA was isolated from tissues using TRIzol reagent (15596018, Thermo Fisher). One
447 µg of RNA was used to synthesize complementary DNA (**cDNA**) using the High-Capacity
448 Reverse Transcription Kit (4368814, Applied Biosystems), followed by a 1:10 dilution in nuclease-
449 free water. Quantitative PCR (**qPCR**) was performed using PowerSYBR Green PCR Master Mix
450 (4367659, Thermo Fisher) and transcript-specific primer sets (250 nM). Primer sequences are
451 provided in Supplemental Material, Tables S5 and S6. qPCR was conducted with a QuantStudio
452 5 Real-Time PCR System (Thermo Fisher) using the following cycling conditions: an initial
453 denaturation step at 95 °C for 10 min, followed by 40 cycles of two-step PCR (95°C for 15 sec,
454 60°C for 1 min). A dissociation curve was then generated with the following steps: 95°C for 15
455 sec, 60°C for 1 min, and a final at 95°C for 15 sec. Relative mRNA expression levels were
456 calculated using the ΔΔCt method. Glyceraldehyde 3-phosphate dehydrogenase (*Gapdh*) and
457 RNA polymerase II subunit A (*POLR2A*) were used as reference genes for rat and human
458 samples, respectively.
459
460 *In situ hybridization*
461 In situ hybridization was performed using paraffin-embedded human placenta and frozen rat
462 placentation site tissue sections and the RNAscope® Multiplex Fluorescent Reagent Kit v2
463 (Advanced Cell Diagnostics) following the manufacturer's instructions. Custom-designed probes
464 were used to detect the following transcripts: human *PPARG* (441691, NM_138712.3, target
465 region: 699–1779), human *NOTUM* (430311, NM_178493.5, target region: 259–814), rat *Pparg*
466 (313251, NM_001145367.1, target region: 305–1932); rat *Krt8* (87304-C2, NM_199370.1, target
467 region: 134–1472), and rat *Prl7b1* (860181-C2, NM_153738.1, target region: 28–900). Nuclei
468 were visualized using DAPI (323108, Advanced Cell Diagnostics). Images were captured using a
469 Zeiss Axio Observer 7 microscope.
470
471 *Immunohistochemistry of placental tissues*
472 Formalin fixed paraffin-embedded human placental tissue sections and frozen rat
473 placentation site sections (10 µm thick) fixed in 4% paraformaldehyde were processed for

474 immunohistochemical analyses. Tissue sections were blocked with 10% goat serum (50062Z,
475 Thermo Fisher) and incubated overnight at 4°C with primary antibodies against vimentin (1:300,
476 sc-6260, Santa Cruz Biotechnology), pan-cytokeratin (1:100, F3418, Sigma-Aldrich), perforin
477 (1:300, TP251, Amsbio), or PPARG (human: 1:100, sc-7273, Santa Cruz Biotechnology; rat:
478 1:100, 2435S, Cell Signaling Technology). Immunostaining was visualized using fluorescence-
479 tagged secondary antibodies: Alexa Fluor 488-conjugated goat anti-mouse IgG (A11001, Thermo
480 Fisher) and Alexa Fluor 568-conjugated goat anti-rabbit IgG (A11011, Thermo Fisher). Sections
481 were counterstained with DAPI, mounted in Fluoromount-G (0100-01, Southern Biotech), and
482 imaged using a Nikon 90i upright microscope equipped with Photometrics CoolSNAP-ES
483 monochrome camera (Roper). Regions of the uterine–placental interface containing cytokeratin-
484 positive cells were quantified using ImageJ software, as previously described (Dominguez et al.
485 2024; Rosario et al. 2008).
486
487 *Immunohistochemistry of trophoblast organoids*
488 Organoids were recovered from Matrigel using Cell Recovery Solution (354253, Corning) and
489 dissociated by gentle pipetting. After 30 min incubation on ice, samples were centrifuged (600 xg,
490 5 min), washed with PBS, and fixed in 4% paraformaldehyde on ice for 30 min. Fixed organoids
491 were suspended in 20% sucrose solution and incubated at 4°C overnight. The sucrose solution
492 was subsequently replaced with 1 mL of warm gelatin/sucrose solution and incubated at 37°C for
493 15 min. Blocks of gelatin containing trophoblast organoids were froze for 1-2 min and stored at-
494 80°C until processed for cryosectioning. Sections were permeabilized in PBS containing 4%
495 bovine serum albumin and 0.5% Triton X-100. Primary antibodies to HLA-G (1:300, phycoerythrin
496 (**PE**)-labeled, ab24384, Abcam), CGB (1:500, ab9528, Abcam) and TP63 (1:500, ab124762,
497 Abcam) were incubated with tissue sections overnight at 4°C, followed by secondary antibody
498 incubation. Sections were counterstained with DAPI, mounted in Fluoromount-G (0100-01,
499 Southern Biotech), and imaged using a Nikon 90i upright microscope equipped with Photometrics
500 CoolSNAP-ES monochrome camera (Roper).
501

502 *Western blotting*

503 Human trophoblast cell lysates were processed using the radioimmunoprecipitation assay
504 lysis buffer (sc-24948A, Santa Cruz Biotechnology) and protein concentrations determined using
505 the DC Protein Assay Kit (5000112, Bio-Rad). Proteins (50 µg/lane) were separated by sodium
506 dodecyl sulfate polyacrylamide gel electrophoresis. Separated proteins were electrophoretically
507 transferred to polyvinylidene difluoride membranes (10600023, GE Healthcare) for 1 h at 25 V on
508 a semi-dry transfer apparatus (Bio-Rad). Membranes were subsequently blocked with 5% milk for
509 1 h at room temperature, followed by incubation with antibodies to PPARG (1:500, 2435S, Cell
510 Signaling Technology or GAPDH (1:5,000, AM4300, Invitrogen) in 5% milk overnight at 4°C. After
511 primary antibody incubation, the membranes were washed in Tris-buffered saline with Tween 20
512 (**TBS-T**) three times (10 min/wash) at room temperature. The membranes were then incubated
513 with anti-mouse immunoglobulin G conjugated to horseradish peroxidase (**HRP**; 1:5000, Cell
514 Signaling Technology) in 5% milk for 1 h at room temperature, washed in TBS-T three times (10
515 min/wash) at room temperature, immersed in Immobilon Crescendo Western HRP Substrate
516 (WBLUR0500, Sigma-Aldrich), and luminescence detected using Chemi Doc MP Imager (Bio-
517 Rad).

518

519 *RNA-seq analysis*

520 Transcript profiles were generated from control and PPARG shRNA treated human CT27 TS
521 cells following EVT cell differentiation. Three independent lentiviral transductions for each shRNA
522 were analyzed. RNA was isolated and integrity assessed using an Agilent 2100 Bioanalyzer.
523 cDNA libraries prepared with Illumina TruSeq RNA preparation kits according to the
524 manufacturer's instructions. Barcoded cDNA libraries were multiplexed onto a TruSeq paired-end
525 flow cell and sequenced (100-bp paired-end reads) with a TruSeq 200-cycle sequencing-by-
526 synthesis kit. Samples were sequenced on an Illumina NovaSeq platform at the KUMC Genome
527 Sequencing Facility. Reads from *.fastq files were mapped to the human reference genome
528 (GRCh37) using CLC Genomics Workbench 12.0 (Qiagen). Transcript abundance was expressed
529 as total reads, and a false discovery rate of 0.05 was used as a cutoff for significant differential

530 expression. Statistical significance was calculated by empirical analysis of digital gene expression
531 followed by Bonferroni's correction.
532
533 *ChIP-seq analysis*
534 PPARG ChIP was performed on human CT27 TS cells following EVT cell differentiation using
535 commercially available SimpleChIP® Enzymatic Chromatin Immunoprecipitation Kit (Magnetic
536 Beads, 9003, Cell Signaling Technology) and PPARG antibody (2435S, Cell Signaling
537 Technology). Three independent replicates were processed. The ChIP-seq library was
538 constructed using the Tecan Ovation Ultralow DNA System V2 (NuGEN Technologies, Redwood
539 City, CA) and sequenced on an Illumina NovaSeq platform. Details of data processing and
540 analyses are presented in Supplemental Material.
541
542 *Statistics*
543 Statistical analyses were performed with GraphPad Prism 10.2.3 software. Statistical
544 comparisons were evaluated using Student's *t* test or one-way analysis of variance with Tukey's
545 or Dunnett's post hoc tests as appropriate. Statistical significance was determined as $P<0.05$.
546
547 *Study approval*
548 All protocols using rats were approved by the University of Kansas Medical Center Animal
549 Care and Use Committee, Kansas City, Kansas (approved protocol 22-01-220).
550
551 *Data available*
552 RNA-seq and ChIP-seq datasets are available at the Gene Expression Omnibus database,
553 https://www.ncbi.nlm.nih.gov/geo/ (GSE302291 and GSE302293). All data generated and
554 analyzed in this study are included in the published article and supporting files.
555
556 *Competing Interest Statement*
557 The authors have declared that no conflict of interest exists.

Acknowledgments

We thank Brandi Miller and Stacy Oxley for administrative assistance. The work was supported by the Lalor Foundation (E.M.D., A.M.-I.), Kansas Idea Network of Biomedical Research Excellence, P20 GM103418 (E.M.D, A.M.-I.), Program of the Joint Usage/Research Center for Developmental Medicine and High Depth Omics, IMEG, Kumamoto University (H.O.), NIH grants: HD115834 (A.M.-I.), HD104071 (K.I.), HD020676 (M.J.S.), HD105734 (M.J.S.), HD112559 (M.J.S., G.T.), and the Sosland Foundation (M.J.S.).

Author Contributions

E.M.D and M.J.S. conceived and designed the research; E.M.D., A.M-I. and A.F. performed experiments; K.I., H.O., and T.A. provided experimental tools for analysis; E.M.D., A.M-I., K.C., G.T., M.P., and M.J.S. analyzed the data and interpreted results of experiments; E.M.D. and M.J.S. prepared the manuscript. All authors read, contributed to editing, and approved the final version of manuscript.

References

Ahmadian M, Suh JM, Hah N, Liddle C, Atkins AR, Downes M, Evans RM. 2013. PPARγ signaling and metabolism: the good, the bad and the future. *Nat Med* **19**: 10.1038/nm.3159.

Ain R, Canham LN, Soares MJ. 2003. Gestation stage-dependent intrauterine trophoblast cell invasion in the rat and mouse: novel endocrine phenotype and regulation. *Dev Biol* **260**: 176–190.

Ain R, Konno T, Canham LN, Soares MJ. 2006. Phenotypic analysis of the rat placenta. *Methods Mol Med* **121**: 295–313.

Asami-Miyagishi R, Iseki S, Usui M, Uchida K, Kubo H, Morita I. 2004. Expression and function of PPARgamma in rat placental development. *Biochem Biophys Res Commun* **315**: 497–501.

Aye ILMH, Tong S, Charnock-Jones DS, Smith GCS. 2025. The human placenta and its role in reproductive outcomes revisited. *Physiol Rev* **105**: 2305–2376.

587 Barak Y, Nelson MC, Ong ES, Jones YZ, Ruiz-Lozano P, Chien KR, Koder A, Evans RM. 1999. PPAR
588 gamma is required for placental, cardiac, and adipose tissue development. *Mol Cell* **4**:
589 585–595.

590 Berger J, Moller DE. 2002. The mechanisms of action of PPARs. *Annu Rev Med* **53**: 409–435.

591 Brosens I, Pijnenborg R, Vercruysse L, Romero R. 2011. The "great obstetrical syndromes" are
592 associated with disorders of deep placentation. *Am J Obstet Gynecol* **204**: 193–201.

593 Brosens I, Puttemans P, Benagiano G. 2019. Placental bed research: I. The placental bed:
594 from spiral arteries remodeling to the great obstetrical syndromes. *Am J Obstet Gynecol*
595 **221**: 437–456.

596 Calkins K, Devaskar SU. 2011. Fetal origins of adult disease. *Curr Probl Pediatr Adolesc Health*
597 *Care* **41**: 158–176.

598 Carter AM, Enders AC. 2004. Comparative aspects of trophoblast development and placentation.
599 *Reprod Biol Endocrinol* **2**: 46.

600 Chakraborty D, Cui W, Rosario GX, Scott RL, Dhakal P, Renaud SJ, Tachibana M, Rumi MAK,
601 Mason CW, Krieg AJ, et al. 2016. HIF-KDM3A-MMP12 regulatory circuit ensures
602 trophoblast plasticity and placental adaptations to hypoxia. *Proc Natl Acad Sci U S A*
603 **113**: E7212–E7221.

604 Chakraborty D, Rumi MAK, Konno T, Soares MJ. 2011. Natural killer cells direct hemochorial
605 placentation by regulating hypoxia-inducible factor dependent trophoblast lineage
606 decisions. *Proc Natl Acad Sci U S A* **108**: 16295–16300.

607 Chang W-L, Liu Y-W, Dang Y-L, Jiang X-X, Xu H, Huang X, Wang Y-L, Wang H, Zhu C, Xue L-Q, et al.
608 2018. PLAC8, a new marker for human interstitial extravillous trophoblast cells,
609 promotes their invasion and migration. *Development* **145**: dev148932.

610 Dhakal P, Soares MJ. 2017. Single Step PCR-Based Genetic Sex Determination for Rat Tissues and
611 Cells. *Biotechniques* **62**: 232–233.

612 Dominguez EM, Moreno-Irusta A, Scott RL, Iqbal K, Soares MJ. 2024. TFAP2C is a key regulator of
613 intrauterine trophoblast cell invasion and deep hemochorial placentation. *JCI Insight* **10**:
614 e186471.

615 Erlebacher A. 2013. Immunology of the maternal-fetal interface. *Annu Rev Immunol* **31**: 387–
616 411.

617 Feige JN, Gelman L, Michalik L, Desvergne B, Wahli W. 2006. From molecular action to
618 physiological outputs: peroxisome proliferator-activated receptors are nuclear receptors
619 at the crossroads of key cellular functions. *Prog Lipid Res* **45**: 120–159.

620 Fisher SJ. 2015. Why is placentation abnormal in preeclampsia? *Am J Obstet Gynecol* **213**: S115–
621 S122.

622 Fournier T, Guibourdenche J, Handschuh K, Tsatsaris V, Rauwel B, Davrinche C, Evain-Brion D.
623 2011. PPARγ and human trophoblast differentiation. *J Reprod Immunol* **90**: 41–49.

624 Fournier T, Tsatsaris V, Handschuh K, Evain-Brion D. 2007. PPARs and the placenta. *Placenta* **28**:
625 65–76.

626 Georgiades P, Ferguson-Smith AC, Burton GJ. 2002. Comparative developmental anatomy of the
627 murine and human definitive placentae. *Placenta* **23**: 3–19.

628 Gluckman PD, Hanson MA, Cooper C, Thornburg KL. 2008. Effect of In Utero and Early-Life
629 Conditions on Adult Health and Disease. *N Engl J Med* **359**: 61–73.

630 Guo Q, Choi J, Lee M, Kim J. 2025. PPARG-centric transcriptional re-wiring during differentiation
631 of human trophoblast stem cells into extravillous trophoblasts. *Nucleic Acids Res* **53**:
632 gkaf669.

633 Harris LK. 2010. Review: Trophoblast-vascular cell interactions in early pregnancy: how to
634 remodel a vessel. *Placenta* **31 Suppl**: S93-98.

635 Harris LK, Benagiano M, D'Elios MM, Brosens I, Benagiano G. 2019. Placental bed research: II.
636 Functional and immunological investigations of the placental bed. *Am J Obstet Gynecol*
637 **221**: 457–469.

638 Hemberger M, Nozaki T, Masutani M, Cross JC. 2003. Differential expression of angiogenic and
639 vasodilatory factors by invasive trophoblast giant cells depending on depth of invasion.
640 *Dev Dyn* **227**: 185–191.

641 Holdsworth-Carson SJ, Lim R, Mitton A, Whitehead C, Rice GE, Permezel M, Lappas M. 2010.
642 Peroxisome proliferator-activated receptors are altered in pathologies of the human
643 placenta: gestational diabetes mellitus, intrauterine growth restriction and
644 preeclampsia. *Placenta* **31**: 222–229.

645 Iqbal K, Dominguez EM, Nixon B, Moreno-Irusta A, Crnkovich B, Scott RL, Vu HTH, Tuteja G,
646 Vivian JL, Soares MJ. 2024. Conditionally mutant animal model for investigating the
647 invasive trophoblast cell lineage. *Development* **151**: dev202239.

648 Jeyarajah MJ, Jaju Bhattad G, Kelly RD, Baines KJ, Jaremek A, Yang F-HP, Okae H, Arima T,
649 Dumeaux V, Renaud SJ. The multifaceted role of GCM1 during trophoblast
650 differentiation in the human placenta. *Proc Natl Acad Sci U S A* **119**: e2203071119.

651 Kadam L, Kohan-Ghadr HR, Drewlo S. 2015. The balancing act – PPAR-γ's roles at the maternal-
652 fetal interface. *Syst Biol Reprod Med* **61**: 65–71.

653 Karvas RM, Khan SA, Verma S, Yin Y, Kulkarni D, Dong C, Park K, Chew B, Sane E, Fischer LA, et al.
654 2022. Stem-cell-derived trophoblast organoids model human placental development
655 and susceptibility to emerging pathogens. *Cell Stem Cell* **29**: 810-825.e8.

656 Kaufmann P, Black S, Huppertz B. 2003. Endovascular trophoblast invasion: implications for the
657 pathogenesis of intrauterine growth retardation and preeclampsia. *Biol Reprod* **69**: 1–7.

658 Kim M, Jang YJ, Lee M, Guo Q, Son AJ, Kakkad NA, Roland AB, Lee B-K, Kim J. 2024. The
659 transcriptional regulatory network modulating human trophoblast stem cells to
660 extravillous trophoblast differentiation. *Nat Commun* **15**: 1285.

661 Kubota N, Terauchi Y, Miki H, Tamemoto H, Yamauchi T, Komeda K, Satoh S, Nakano R, Ishii C,
662 Sugiyama T, et al. 1999. PPAR gamma mediates high-fat diet-induced adipocyte
663 hypertrophy and insulin resistance. *Mol Cell* **4**: 597–609.

664 Kuna M, Dhakal P, Iqbal K, Dominguez EM, Kent LN, Muto M, Moreno-Irusta A, Kozai K, Varberg
665 KM, Okae H, et al. CITED2 is a conserved regulator of the uterine–placental interface.
666 *Proc Natl Acad Sci U S A* **120**: e2213622120.

667 Liu Y, Fan X, Wang R, Lu X, Dang Y-L, Wang H, Lin H-Y, Zhu C, Ge H, Cross JC, et al. 2018. Single-
668 cell RNA-seq reveals the diversity of trophoblast subtypes and patterns of differentiation
669 in the human placenta. *Cell Res* **28**: 819–832.

670 Maltepe E, Fisher SJ. 2015. Placenta: the forgotten organ. *Annu Rev Cell Dev Biol* **31**: 523–552.

671 Meinhardt G, Waldhäusl H, Lackner AI, Wächter J, Maxian T, Höbler A-L, Vondra S, Kunihs V,
672 Saleh L, Haslinger P, et al. The multifaceted roles of the transcriptional coactivator TAZ
673 in extravillous trophoblast development of the human placenta. *Proc Natl Acad Sci U S A*
674 **122**: e2426385122.

675 Muto M, Chakraborty D, Varberg KM, Moreno-Irusta A, Iqbal K, Scott RL, McNally RP, Choudhury
676 RH, Aplin JD, Okae H, et al. 2021. Intersection of regulatory pathways controlling
677 hemostasis and hemochorial placentation. *Proc Natl Acad Sci U S A* **118**: e2111267118.

678 Okae H, Toh H, Sato T, Hiura H, Takahashi S, Shirane K, Kabayama Y, Suyama M, Sasaki H, Arima
679 T. 2018. Derivation of Human Trophoblast Stem Cells. *Cell Stem Cell* **22**: 50-63.e6.

680 Parast MM, Yu H, Ciric A, Salata MW, Davis V, Milstone DS. 2009. PPARγ Regulates Trophoblast
681 Proliferation and Promotes Labyrinthine Trilineage Differentiation ed. S.K. Dey. *PLoS*
682 *ONE* **4**: e8055.

683 Pavan L, Tarrade A, Hermouet A, Delouis C, Titeux M, Vidaud M, Thérond P, Evain-Brion D,
684 Fournier T. 2003. Human invasive trophoblasts transformed with simian virus 40 provide
685 a new tool to study the role of PPARγ in cell invasion process. *Carcinogenesis* **24**: 1325–
686 1336.

687 Pijnenborg R, Robertson WB, Brosens I, Dixon G. 1981. Review article: trophoblast invasion and
688 the establishment of haemochorial placentation in man and laboratory animals.
689 *Placenta* **2**: 71–91.

690 Pijnenborg R, Vercruysse L, Hanssens M. 2006. The uterine spiral arteries in human pregnancy:
691 facts and controversies. *Placenta* **27**: 939–958.

692 Rai A, Cross JC. 2014. Development of the hemochorial maternal vascular spaces in the placenta
693 through endothelial and vasculogenic mimicry. *Dev Biol* **387**: 131–141.

694 Rätsep MT, Felker AM, Kay VR, Tolusso L, Hofmann AP, Croy BA. 2015. Uterine natural killer
695 cells: supervisors of vasculature construction in early decidua basalis. *Reproduction* **149**:
696 R91-102.

697 Renaud SJ, Scott RL, Chakraborty D, Rumi MAK, Soares MJ. 2017. Natural killer-cell deficiency
698 alters placental development in rats. *Biol Reprod* **96**: 145–158.

699 Roberts RM, Green JA, Schulz LC. 2016. The evolution of the placenta. *Reproduction* **152**: R179-
700 189.

701 Rodie VA, Young A, Jordan F, Sattar N, Greer IA, Freeman DJ. 2005. Human placental peroxisome
702 proliferator-activated receptor delta and gamma expression in healthy pregnancy and in
703 preeclampsia and intrauterine growth restriction. *J Soc Gynecol Investig* **12**: 320–329.

704 Rosario GX, Konno T, Soares MJ. 2008. Maternal hypoxia activates endovascular trophoblast cell
705 invasion. *Dev Biol* **314**: 362–375.

706 Sauer S. 2015. Ligands for the Nuclear Peroxisome Proliferator-Activated Receptor Gamma.
707 *Trends Pharmacol Sci* **36**: 688–704.

708 Schaiff WT, Barak Y, Sadovsky Y. 2006. The pleiotropic function of PPARγ in the placenta.
709 *Molecular and Cellular Endocrinology* **249**: 10–15.

710 Schaiff WT, Bildirici I, Cheong M, Chern PL, Nelson DM, Sadovsky Y. 2005. Peroxisome
711 proliferator-activated receptor-gamma and retinoid X receptor signaling regulate fatty
712 acid uptake by primary human placental trophoblasts. *J Clin Endocrinol Metab* **90**: 4267–
713 4275.

714 Schaiff WT, Carlson MG, Smith SD, Levy R, Nelson DM, Sadovsky Y. 2000. Peroxisome
715 proliferator-activated receptor-gamma modulates differentiation of human trophoblast
716 in a ligand-specific manner. *J Clin Endocrinol Metab* **85**: 3874–3881.

717 Scott RL, Vu HTH, Jain A, Iqbal K, Tuteja G, Soares MJ. 2022. Conservation at the uterine–
718 placental interface. *Proceedings of the National Academy of Sciences* **119**: e2210633119.

719 Shalom-Barak T, Nicholas JM, Wang Y, Zhang X, Ong ES, Young TH, Gendler SJ, Evans RM, Barak
720 Y. 2004. Peroxisome proliferator-activated receptor gamma controls Muc1 transcription
721 in trophoblasts. *Mol Cell Biol* **24**: 10661–10669.

722 Shimizu T, Oike A, Kobayashi EH, Sekiya A, Kobayashi N, Shibata S, Hamada H, Saito M, Yaegashi
723 N, Suyama M, et al. 2023. CRISPR screening in human trophoblast stem cells reveals
724 both shared and distinct aspects of human and mouse placental development.
725 *Proceedings of the National Academy of Sciences* **120**: e2311372120.

726 Shukla V, Moreno-Irusta A, Varberg KM, Kuna M, Iqbal K, Galligos AM, Aplin JD, Choudhury RH,
727 Okae H, Arima T, et al. 2024. NOTUM-mediated WNT silencing drives extravillous
728 trophoblast cell lineage development. *Proc Natl Acad Sci U S A* **121**: e2403003121.

729 Shukla V, Soares MJ. 2022. Modeling Trophoblast Cell-Guided Uterine Spiral Artery
730 Transformation in the Rat. *Int J Mol Sci* **23**: 2947.

731 Soares MJ, Chakraborty D, Karim Rumi MA, Konno T, Renaud SJ. 2012. Rat placentation: an
732 experimental model for investigating the hemochorial maternal-fetal interface. *Placenta*
733 **33**: 233–243.

734 Soares MJ, Varberg KM, Iqbal K. 2018. Hemochorial placentation: development, function, and
735 adaptations. *Biol Reprod* **99**: 196–211.

736 Tarrade A. 2001. PPAR /RXR Heterodimers Control Human Trophoblast Invasion. *Journal of*
737 *Clinical Endocrinology & Metabolism* **86**: 5017–5024.

738 Tarrade A, Schoonjans K, Guibourdenche J, Bidart JM, Vidaud M, Auwerx J, Rochette-Egly C,
739 Evain-Brion D. 2001. PPARγ/RXRα Heterodimers Are Involved in Human CGβ Synthesis
740 and Human Trophoblast Differentiation. *Endocrinology* **142**: 4504–4514.

741 Varberg KM, Dominguez EM, Koseva B, Varberg JM, McNally RP, Moreno-Irusta A, Wesley ER,
742 Iqbal K, Cheung WA, Schwendinger-Schreck C, et al. 2023. Extravillous trophoblast cell
743 lineage development is associated with active remodeling of the chromatin landscape.
744 *Nat Commun* **14**: 4826.

745 Varberg KM, Iqbal K, Muto M, Simon ME, Scott RL, Kozai K, Choudhury RH, Aplin JD, Biswell R,
746 Gibson M, et al. 2021. ASCL2 reciprocally controls key trophoblast lineage decisions
747 during hemochorial placenta development. *Proc Natl Acad Sci U S A* **118**: e2016517118.

748 Velicky P, Knöfler M, Pollheimer J. 2015. Function and control of human invasive trophoblast
749 subtypes: Intrinsic vs. maternal control. *Cell Adh Migr* **10**: 154–162.

750 Vento-Tormo R, Efremova M, Botting RA, Turco MY, Vento-Tormo M, Meyer KB, Park J-E,
751 Stephenson E, Polański K, Goncalves A, et al. 2018. Single-cell reconstruction of the early
752 maternal-fetal interface in humans. *Nature* **563**: 347–353.

753 Vu HTH, Scott RL, Iqbal K, Soares MJ, Tuteja G. 2023. Core conserved transcriptional regulatory
754 networks define the invasive trophoblast cell lineage. *Development* **150**: dev201826.

755 Waite LL, Louie RE, Taylor RN. 2005. Circulating Activators of Peroxisome Proliferator-Activated
756 Receptors Are Reduced in Preeclamptic Pregnancy. *The Journal of Clinical Endocrinology*
757 *& Metabolism* **90**: 620–626.

758 Waite LL, Person EC, Zhou Y, Lim KH, Scanlan TS, Taylor RN. 2000. Placental peroxisome
759 proliferator-activated receptor-gamma is up-regulated by pregnancy serum. *J Clin*
760 *Endocrinol Metab* **85**: 3808–3814.

761 Wang L-J, Chen C-P, Lee Y-S, Ng P-S, Chang G-D, Pao Y-H, Lo H-F, Peng C-H, Cheong M-L, Chen H.
762 2022. Functional antagonism between ΔNp63α and GCM1 regulates human trophoblast
763 stemness and differentiation. *Nat Commun* **13**: 1626.

764 Wiemers DO, Ain R, Ohboshi S, Soares MJ. 2003. Migratory trophoblast cells express a newly
765 identified member of the prolactin gene family. *J Endocrinol* **179**: 335–346.

766 Xie J, Xu Y, Wan L, Wang P, Wang M, Dong M. 2018. Involvement of follistatin-like 3 in
767 preeclampsia. *Biochem Biophys Res Commun* **506**: 692–697.

768

769

770 **Figures**

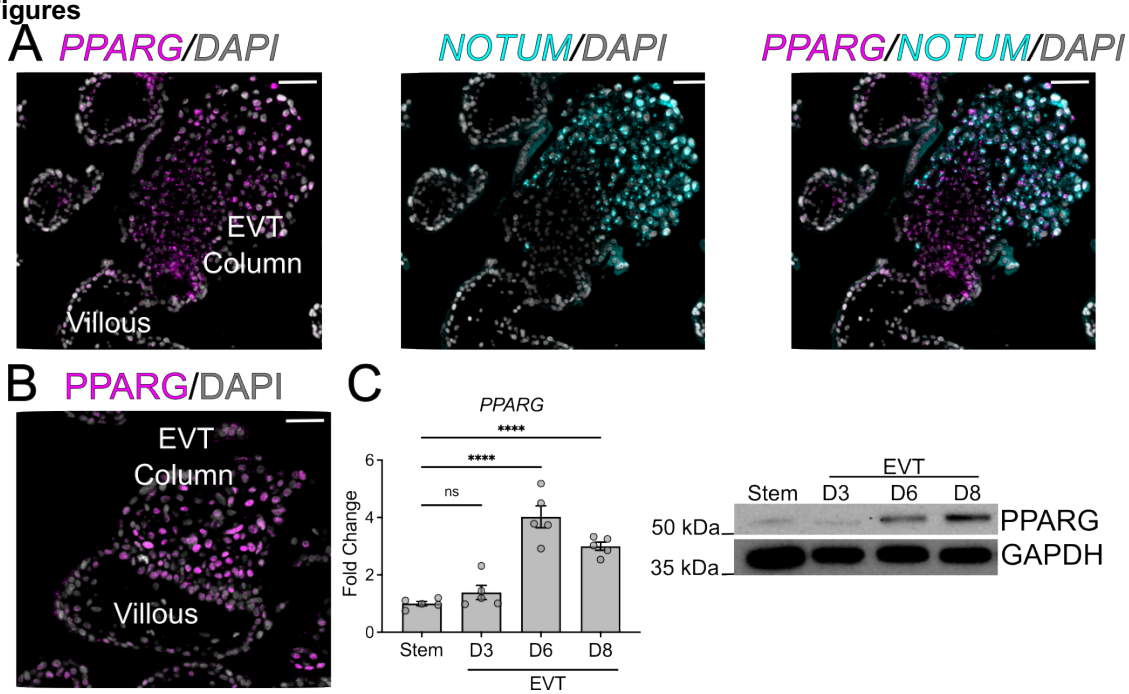

771
772 **Figure 1. PPARG is expressed in EVT cells. A**) *PPARG* transcript (magenta) was localized
773 throughout the EVT column in first trimester human placenta (12 weeks) using in situ
774 hybridization. *NOTUM* (cyan) was used as a distal EVT cell specific transcript. **B**) PPARG
775 immunohistochemistry (magenta) showed nuclear localization within cells of the first trimester
776 EVT cell column (12 weeks). Scale bars for panels A and B=500 µm. **C**) In vitro *PPARG* transcript
777 and protein expression in CT27 (X,X) TS cells in the stem state, day 3 (D3), day 6 (D6), and day
778 8 (D8) of EVT cell differentiation (n=5). Data are presented as mean ± standard error of the
779 mean. Each data point represents a biological replicate. Statistical analysis was performed using
780 ANOVA followed by Tukey's post hoc test: ****p<0.0001.
781

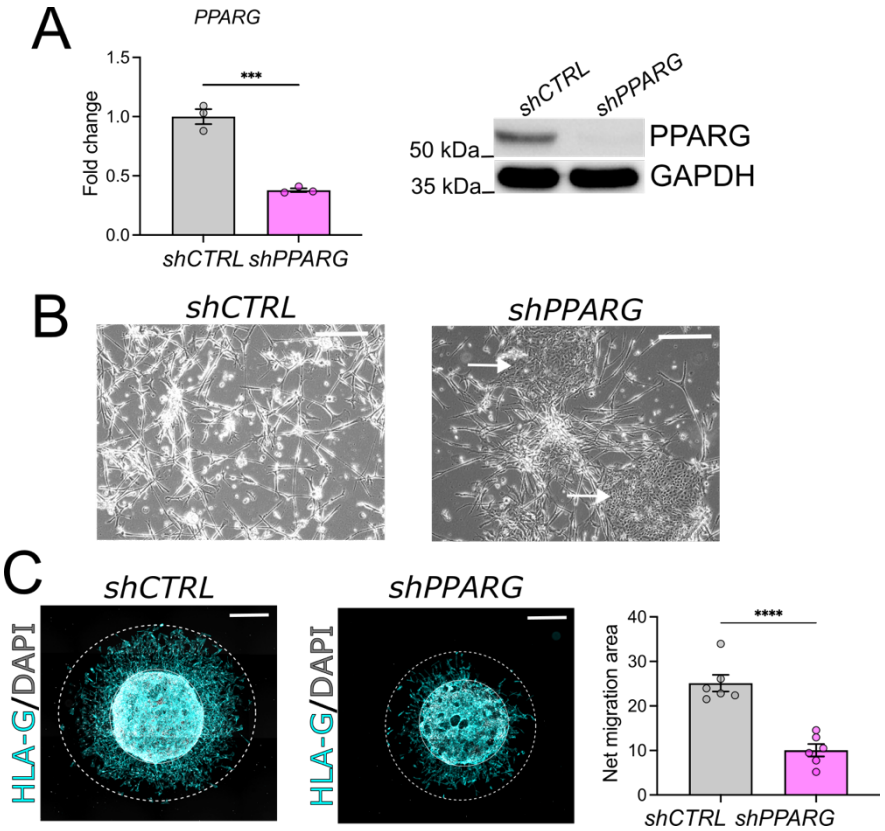

Figure 2. PPARG regulates EVT cell differentiation. A) In vitro *PPARG* transcript and protein levels after 8 days of EVT cell differentiation in control versus PPARG shRNA-treated cells (n=3). B) Phase-contrast images showing the morphology of EVT cells expressing control or PPARG shRNAs. The arrow indicates a cluster of cells exhibiting a stem-like morphology, scale bar=100 µm. C) HLA-G immunofluorescence detection of cell migration in control versus PPARG shRNA-treated cells (n=6), scale bar=500 µm. Data are presented as the mean ± standard error of the mean. Each data point represents a biological replicate. Statistical analysis was performed using unpaired t-tests: ***p<0.001, ****p<0.0001.

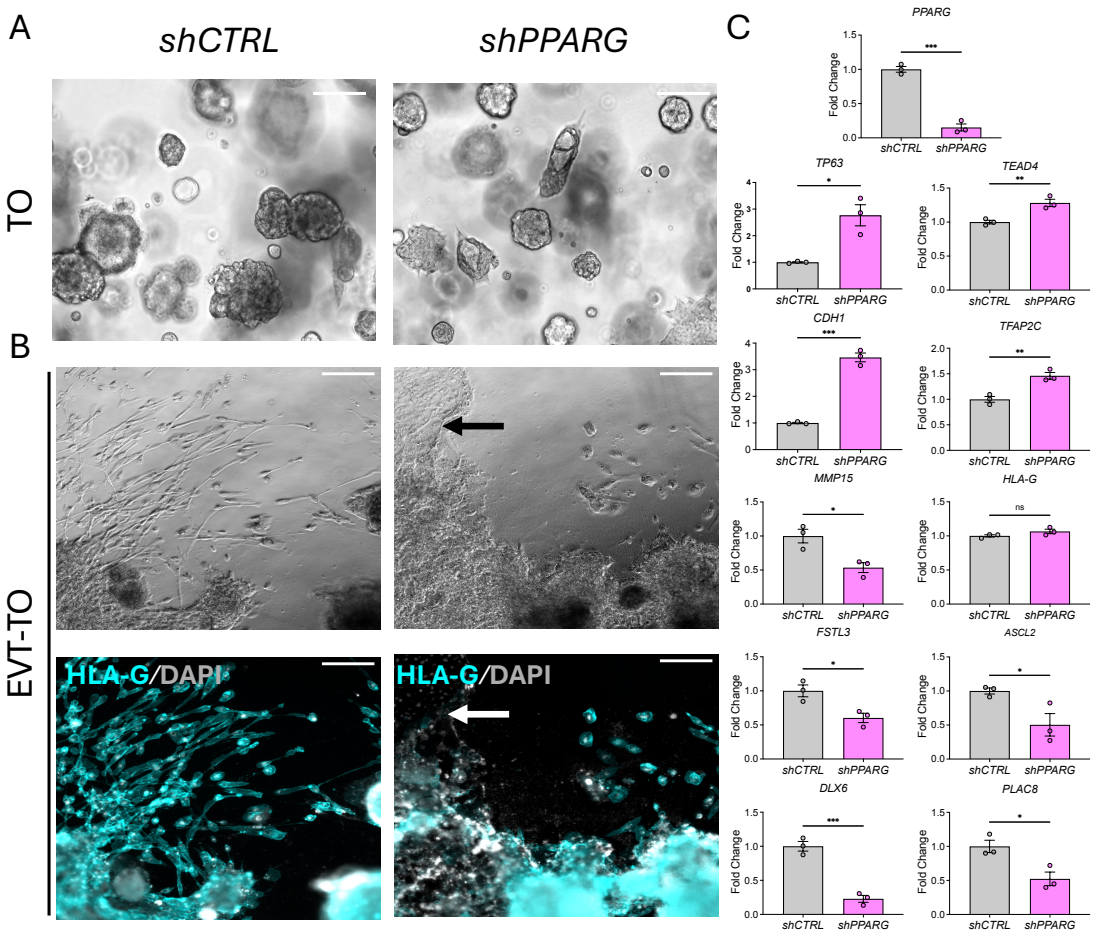

792

793 **Figure 3. Examination of the role of PPARG in EVT cell differentiation using trophoblast**
794 **organoids**. **A**) Phase-contrast images of trophoblast organoids (**TO**) expressing control
795 (**shCTRL**) and PPARG (**shPPARG**) shRNAs, scale bar=100 µm. **B**) Phase-contrast (top panel)
796 and HLA-G immunostaining (bottom panel) images of shCTRL and shPPARG TO transferred to
797 EVT cell differentiation conditions (**EVT-TO**). Arrows indicate the location of cells exhibiting stem-
798 like morphology, scale bar=100. **C**) RT-qPCR analysis of shCTRL and shPPARG TO exposed to
799 EVT cell differentiation conditions. Data are presented as the mean ± standard error of the mean.
800 Each data point represents a biological replicate. Statistical analysis was performed using
801 unpaired t-tests: *P<0.05, **p<0.01, ***p<0.001.
802

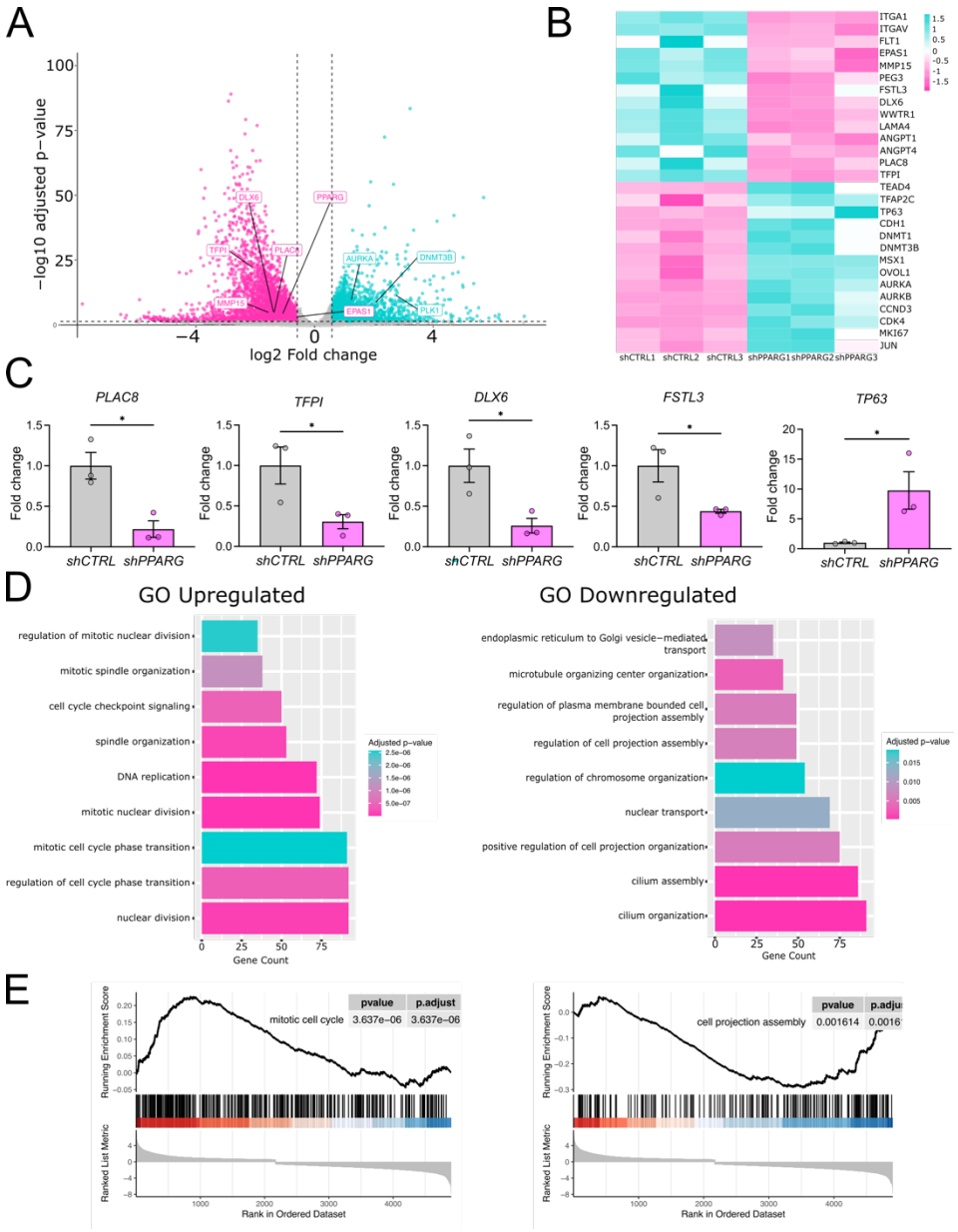

Figure 4. Effects of PPARG on the EVT cell transcriptome. A) Volcano plot and (**B**) heat map depicting RNA-seq analysis of control shRNA and PPARG shRNA for cells exposed to culture conditions used to promote EVT cell differentiation (n=3 per group). Downregulated transcripts are represented by magenta dots ($p<0.05$, fold change<1.5) and cyan dots represent upregulated transcripts ($p<0.05$, fold change>1.5). Z-scores of totals read values are represented in the heat map. **C**) RT-qPCR validation of putative PPARG targets in control and PPARG shRNA treated cells. **D**). Gene ontology (GO) analyses of upregulated and downregulated genes in control and PPARG shRNA treated TS cells exposed to culture conditions used to promote EVT cell differentiation. **E**) Gene set enrichment analyses of upregulated and downregulated genes in control and PPARG shRNA treated TS cells exposed to culture conditions used to promote EVT cell differentiation. CT27 (X,X) TS cell line was used for all experiments shown. Data are presented as the mean ± standard error of the mean. Each data point represents a biological replicate. Statistical analyses were performed using unpaired t-tests: *$p<0.05$.

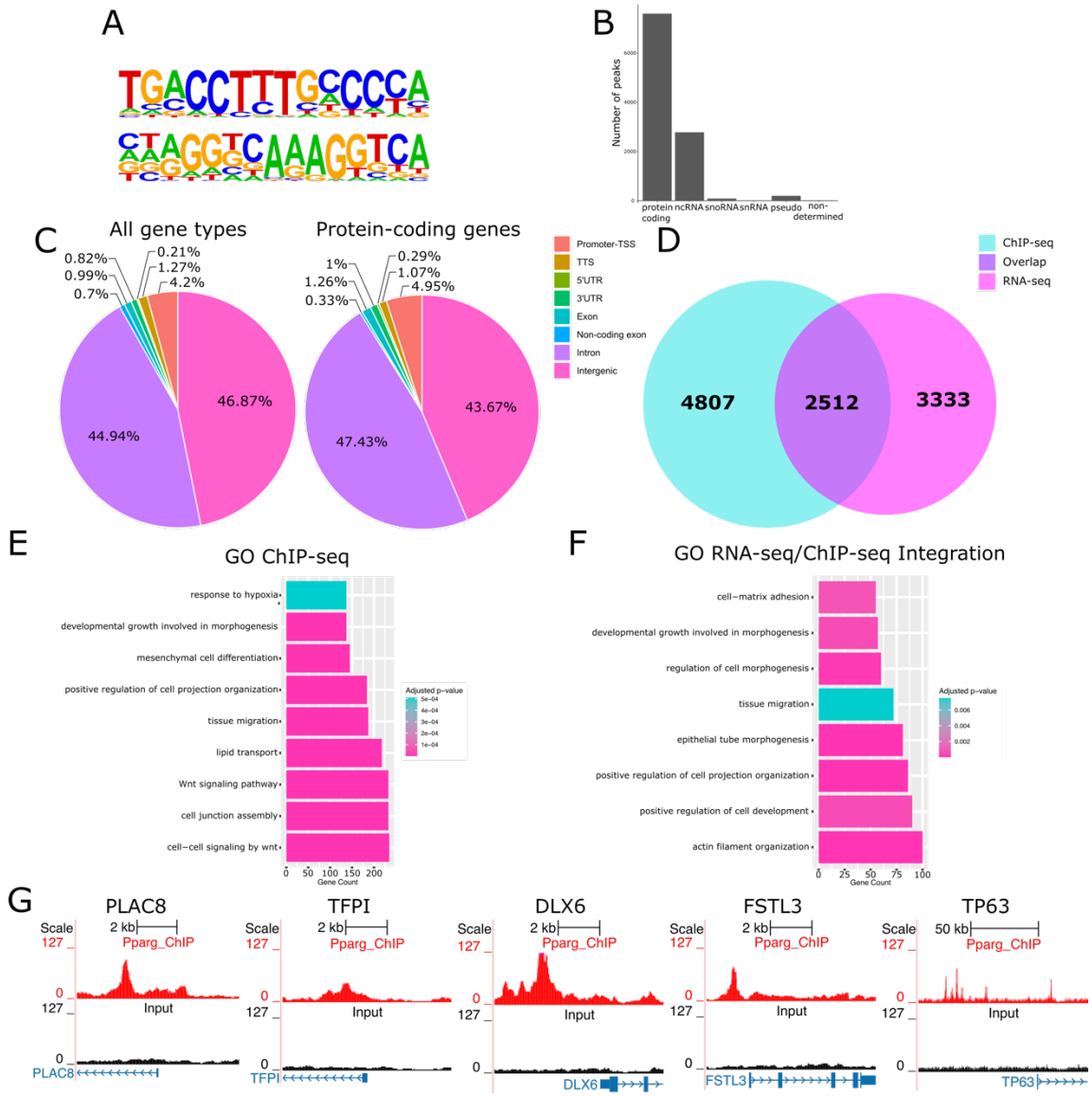

Figure 5. PPARG targets within the EVT cell genome identified using ChIP-seq. A) Two significantly enriched PPARG binding motifs were observed within PPARG ChIP-seq peaks. **B**) Number of peaks observed within specific locations of the genome. **C**) Pie chart showing the distribution of PPARG peaks in genomic regions for all genes and protein-coding genes. **D**) Venn diagram showing the integration of PPARG responsive genes identified by RNA-seq of EVT cells (**see Fig. 4**) and PPARG gene targets identified by PPARG ChIP-seq from EVT cells. **E**) Gene ontology (**GO**) analysis of the PPARG ChIP-seq dataset performed on EVT cells. **F**) GO analysis of an integrated dataset generated from PPARG responsive genes identified by RNA-seq of EVT cells (**see Fig. 4**) and PPARG gene targets identified by PPARG ChIP-seq from EVT cells. **G**) PPARG ChIP-Seq peaks at selected gene loci that exhibit sensitivity to PPARG inhibition. Visualization was performed using the University of California at Santa Cruz Genome browser. Red peaks represent PPARG bound regions, whereas black peaks represent the input DNA.

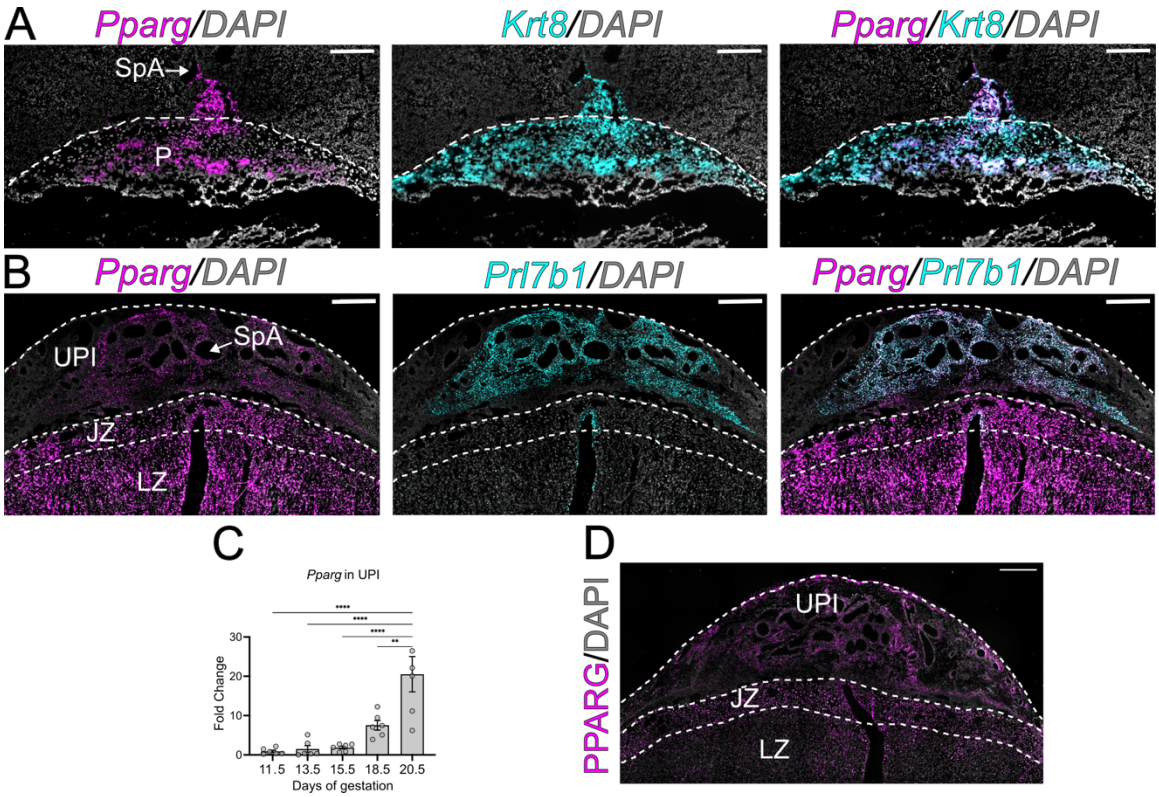

832

833 **Figure 6. Distribution of *Pparg* transcripts and protein in rat placental tissues.** *Pparg*
834 transcripts were localized within rat placentation sites using in situ hybridization. **A**) *Pparg*
835 transcripts (magenta) were co-localized with *Krt8* transcripts (cyan) at gestation day (**gd**) 11.5. **B**)
836 Co-localization of *Pparg* (magenta) and *Prl7b1* (cyan) transcripts within the gd 18.5 placentation
837 site. **C**) RT-qPCR measurement of *Pparg* transcript levels in uterine-placental interface tissues at
838 gd 11.5, 13.5, 15.5, 18.5, and 20.5. Data are presented as mean ± standard error of the mean.
839 Each data point represents a biological replicate from six independent pregnancies (n=6).
840 Statistical analyses were performed with unpaired *t*-tests: **p<0.01, ****p<0.0001. **D**)
841 Immunohistochemical localization of PPARG protein within the gd 18.5 rat uterine-placental
842 interface. Scale bars for panels A, B and D=500 µm. Abbreviations: SpA, spiral artery; UPI,
843 uterine-placental interface; P, placenta; JZ, junctional zone; LZ, labyrinth zone.
844

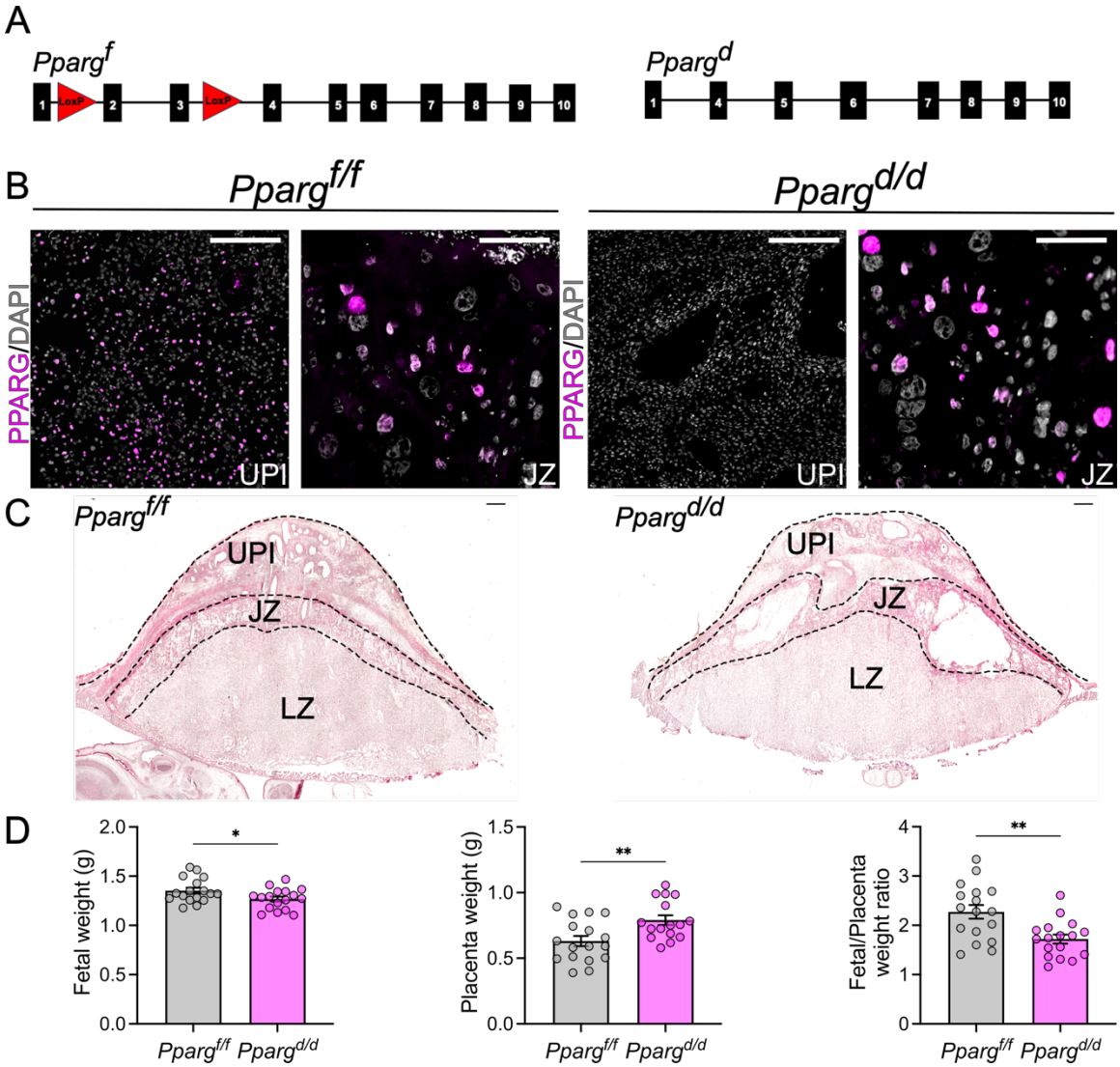

Figure 7. Rat invasive trophoblast-specific deletion of *Pparg*. A) Schematic representation of loxP sites flanking Exons 2 and 3 of the *Pparg* gene and their conditional deletion following Cre recombinase activity driven by *Prl7b1* regulatory DNA. **B**) PPARG immunostaining of *Pparg*$^{f/f}$ and *Pparg*$^{d/d}$ gestation day (**gd**) 18.5 placentation sites. Images show uterine-placental interface tissues (left) and junctional zone tissues (right) for each group, scale bar=50 µm. **C**) Hematoxylin and eosin staining of *Pparg*$^{f/f}$ and *Pparg*$^{d/d}$ gd 18.5 placentation sites, scale bar=500 µm. **D**) Placental weight, fetal weight, and fetal-to-placental weight ratio from gd 18.5 *Pparg*$^{f/f}$ and *Pparg*$^{d/d}$ conceptuses. Data are presented as mean ± standard error of the mean. Each data point represents a biological replicate from six pregnancies (*Pparg*$^{f/f}$, n=17, *Pparg*$^{d/d}$, n=17). Statistical analyses were performed using unpaired *t*-tests: *p<0.05, **p<0.01. Abbreviations: SpA, spiral artery; UPI, uterine-placental interface; JZ, junctional zone; LZ, labyrinth zone.

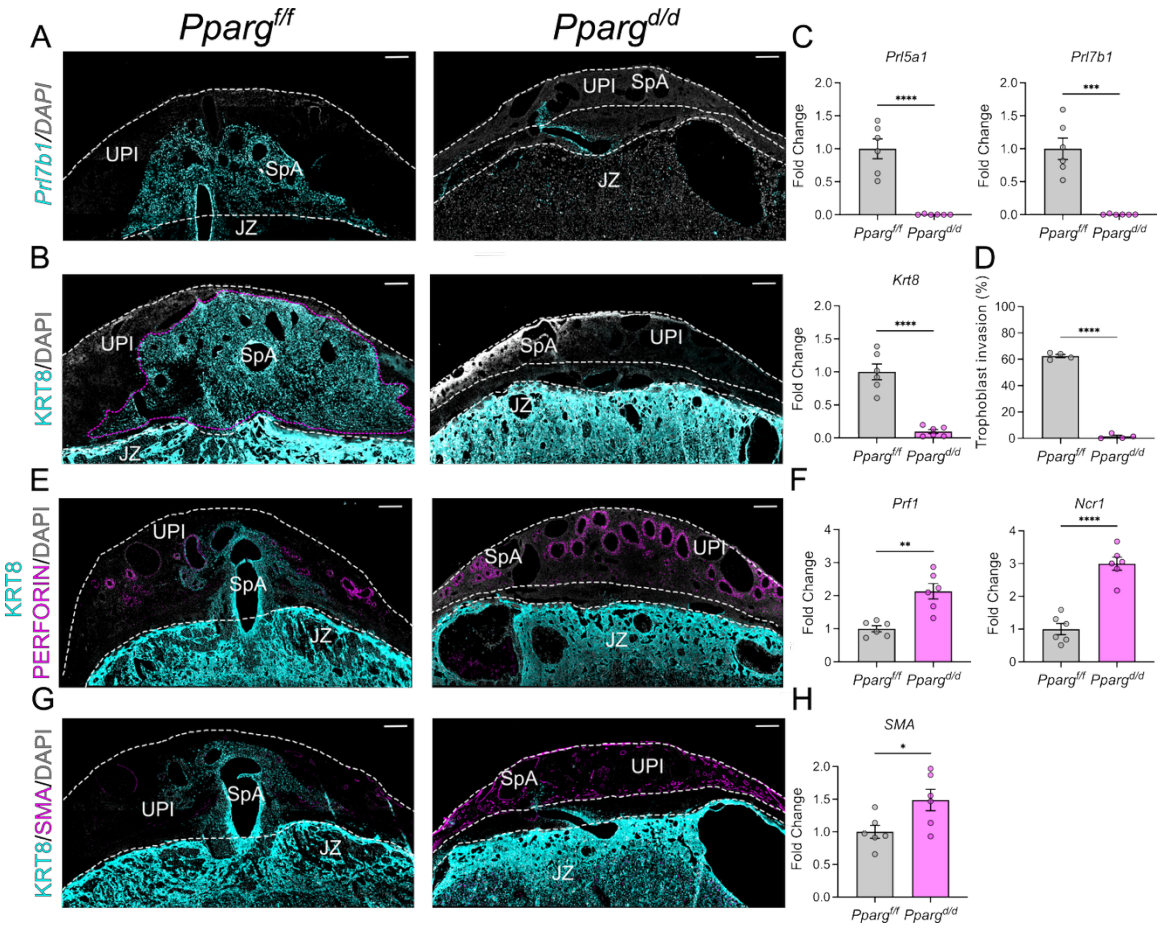

Figure 8. Invasive trophoblast cell-specific *Pparg* disruption impacts pregnancy-dependent transformation of the uterine-placental interface. A) *In situ* hybridization showing *Prl7b1* transcripts (cyan) in gestation day (**gd**) 18.5 *Pparg*$^{f/f}$ and *Pparg*$^{d/d}$ placentation sites. **B**) Immunohistochemical localization of KRT8 (cyan) in gd 18.5 *Pparg*$^{f/f}$ and *Pparg*$^{d/d}$ placentation sites. **C**) RT-qPCR analysis of *Prl7b1, Prl5a1, and Krt8* expression in the uterine-placental interface of gd 18.5 *Pparg*$^{f/f}$ and *Pparg*$^{d/d}$ placentation sites (n=6). **D**) Quantification of trophoblast cell invasion area (magenta dotted line) (n=4). **E**) Immunohistochemical localization of perforin (**PRF1**), a natural killer (**NK**) cell-associated protein, (magenta) and KRT8 (cyan). **F**) RT-qPCR analysis of NK cell-associated transcripts (*Prf1* and *Ncr1*) in the uterine-placental interface of gd 18.5 *Pparg*$^{f/f}$ and *Pparg*$^{d/d}$ placentation sites (n=6). **G**) Immunohistochemical localization of smooth muscle actin (**SMA**, magenta) and KRT8 (cyan) in the uterine-placental interface of gd 18.5 *Pparg*$^{f/f}$ and *Pparg*$^{d/d}$ placentation sites. **H**) RT-qPCR analysis of *Sma* transcript in the uterine-placental interface of gd 18.5 *Pparg*$^{f/f}$ and *Pparg*$^{d/d}$ placentation sites (n=6). Scale bars for images in panels A, B, E and G=500 µm. Data are presented as mean ± standard error of the mean. Each data point represents a distinct uterine-placental interface sample obtained from four to six pregnancies. Statistical analyses were performed using unpaired *t*-tests: **p*<0.05, **p<0.01, ****p*<0.001, *****p*<0.0001. Abbreviations: UPI, uterine-placental interface; JZ, junctional zone; LZ, labyrinth zone; SpA, spiral artery.